DESIGN AND SIMULATION OF PLASMONIC WAVEGUIDE WITH PERIODIC CORRUGATIONS

by

Mohammad Rakeen Niaz(122418)
Mirza Muntasir Nishat(122406)
Mohammad Arif Hossain(122408)

A Thesis Submitted to the Academic Faculty in Partial Fulfillment of the Requirements for the Degree of

BACHELOR OF SCIENCE IN ELECTRICAL AND ELECTRONIC ENGINEERING

Department of Electrical and Electronic Engineering
Islamic University of Technology (IUT)
Gazipur, Bangladesh

November 2016

Declaration of Authorship

We, Mohammad Rakeen Niaz (122418), Mirza Muntasir Nishat (122406) and Mohammad Arif Hossain (122408), declare that this thesis titled, 'Design and Simulation of Plasmonic Waveguide with Periodic Corrugations' and the works presented in it are our own. We confirm that:

- This work has been done for the partial fulfillment of the Bachelor of Science in Electrical and Electronic Engineering degree at this university.
- Any part of this thesis has not been submitted anywhere else for obtaining any degree.
- Where we have consulted the published work of others, we have always clearly attributed the sources.

Submitted By:

_____

Mohammad Rakeen Niaz(122418)

_____

Mirza Muntasir Nishat(122406)

_____

Mohammad Arif Hossain(122408)

Abstract

The key performance parameters of an MIM(metal-insulator-metal) surface plasmonic waveguide having periodic corrugations has been investigated. The transmittance, taking into account a wide range of optical wavelength was demonstrated by rigorous numerical calculations against the variation of different structural aspects. The results indicate that a very satisfactory filtering characteristic can be achieved by this variation of the parameters The output of this investigation has the potential to develop ultra-compact photonic filters for higher integration.

Acknowledgement

We would first like to thank my thesis supervisor Rakibul Hasan Sagor , Assistant Professor at Islamic University of Technology(IUT). He was always co-operative whenever we ran into trouble or had a question about our research or writing. He consistently allowed this paper to be our own work, but steered us in the right the direction whenever he thought we needed it.

We would also like to acknowledge Mirza Fuad Adnan, Lecturer at Islamic University of Technology as the co-supervisor of this thesis, and we are gratefully indebted to his very valuable contribution to this thesis.

We are also indebted to all the faculty members of IUT who have been a constant source of encouragement and enthusiasm during this thesis project.

Finally, oue deepest gratitude goes to our families for their unflagging love and unconditional support throughout our lives and our studies. You made us live the most unique, magic and carefree childhood that has made us who we are now!

Table of Contents

List of figures

Chapter 1

Introduction

In metals, light can couple to electrons to form a wave that is bound to the surface of the metal. This wave is called the surface plasmon. The surface plasmon mode is generally characterized by intense fields that decay exponentially away from the interface between the metal and the surrounding environment. Surface plasmons display very important properties, including strongly enhanced local fields; tremendous sensitivity to changes in the local environment; and the ability to localize energy to tiny volumes not restricted by the wavelength of the exciting light.

Plasmonics have become one of the most attractive research interest in present times. Its ability to overcome the diffraction limit has made it such attractive[1-3].This ability has provided three major advantages, namely faster speed of operation, smaller devices, less power consumption. Other probable applications of surface plasmon polariton(SPP) includes sub-wavelength imaging[4, 5], Bragg's reflector[6], bio-sensing[7], meta materials[8] and also can be implemented in solar cells[9, 10]. Photons travelling on optical fibres or thin film will be used in those optical processors making the system lighter and more compact[11].

Due to their unique properties, plasmons have found a broad range of applications in various areas of science. In chemistry and biology for example, the sensitivity of surface plasmons is used to form the basis for powerful chemical and biochemical detectors that can monitor molecular binding events. In optics, the large field strengths of surface plasmons can dramatically enhance a variety of phenomena such as Raman scattering and light transmission through sub-wavelength apertures. In addition, the size of certain SPP configurations can be smaller than the operation

wavelength, thus offering a path to decrease the size of optical components beyond the diffraction limit.

MIM [12] structures provide higher confinement on the other hand IMI[13, 14] structures facilitate longer propagation length. Relentless research is going on to investigate the tradeoff between confinement and propagation loss. For small corrugations losses are found to be very low while a high loss is expected with the gradual enlargement of corrugations[13][14][15]. Photonic crystal fiber, nonlinear photonic crystal and photonic bandgap microcavities[16-19] have been designed so far. Plasmonic waveguide designing has become a prominent domain where the researchers are working at length. Jia et al [20] have proposed a nanoplasmonic high pass wavelength filter based on an MIM waveguide. Asanka et al.[21] have designed an improved transmission model for MDM waveguide with stub structure. Binfeng et al. [22]have reported an analysis of a nanoscale plasmonic filter on a rectangular MIM waveguide.

1.1: Brief Introduction of Surface Plasmon Polariton

Surface Plasmon Polaritons (SPPs) are electromagnetic surface waves confined to the interface of two materials with dielectric functions of opposite signs, i.e. metal / dielectric. They occur as a result of a resonant interaction between an illuminating electromagnetic wave and a collective surface electron density oscillation of the free electrons of the conductor.

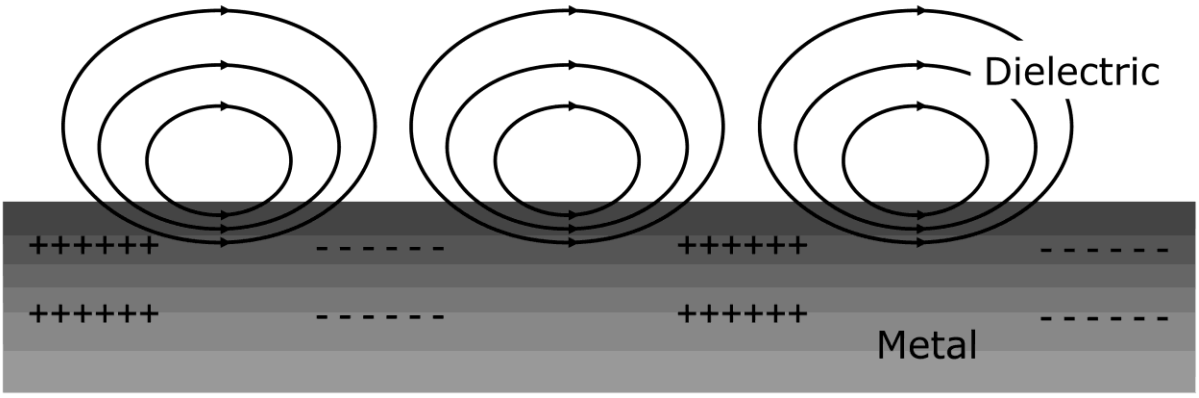

[Fig. 1.1] Illustration of SP **E** fields coupled to electron density oscillations, at a metal / dielectric half space.

1.2: Literature Review

Since the late 1950's, research on the topic of surface plasmons has grown steadily, receiving a number of important growth boosts along the way. In particular, landmark articles by Ritchie [1], Kretschmann [2] and Otto [3] in the late 1950's and 1960's sparked an interest in other researchers to join the field - not only from a fundamental physics research point of view, but also with the realisation of the potential that SPPs offer to other fields; for example as the foundations for molecular biosensors. Another major expansion to the field arrived in the mid 1990's, when the availability of new nanoscale fabrication technologies created previously un-accessible opportunities to control SPP properties. This enabled researchers to tailor design surface topographies on the nanoscale which revealed new aspects of their underlying science, and in-doing so, inspired and encouraged new groups to join the ever-growing field of plasmonics.

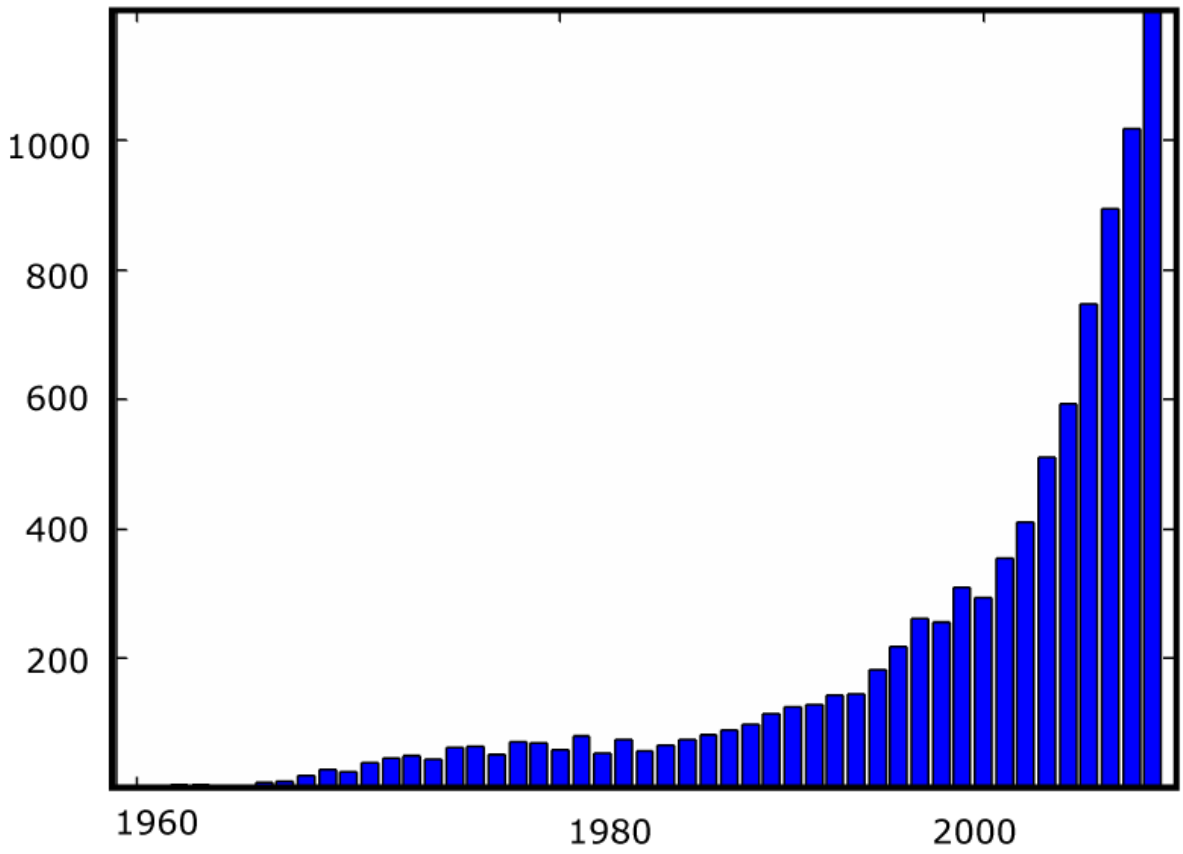

[Fig. 1.2] Number of papers containing “surface plasmon” in the title from 1960 to 2008 [4].

These points are emphasised in [Fig. 2], which displays the number of published articles containing the phrase “surface plasmon” in the title in a given year [4].

Although this is not an exact count of the number of papers dealing with research in the field, it is a good indication of its growth from 1960, when Stern and Ferrell first dubbed the term “Surface Plasmon” (from “surface plasma oscillation”) . Although it was the middle of the 20th century that marked the beginning of direct research on SPs, properties of SPPs have been taken advantage of long before the onset of scientific plasmon research. (Note: SPs differs slightly in definition from SPPs (a term introduced in 1974), where ‘polariton’ indicates a coupled oscillation of bound electrons and light at a metallic interface]

The parameters of several metals have been reported to our knowledge. Jin et al.[23] determined the modified Debye model parameters for gold which are applicable in the wavelength range of 550-950 nm. Krug et al. [24] reported the gold parameters that are applicable in the wavelength range of 700-1000 nm. W.H.P. Pernice et al.[25] extracted the parameters for Nickel using Lorentz-Drude model. A.D. Rakic et al.[26] reported the parameters for Nickel, Palladium, Titanium and 8 other metals using Lorentz-Drude and Brendel-Bormann Model. M.A. Ordal et al.[27] extracted the parameters for fourteen metals in the infrared and far-infrared range.

Bends, splitters and recombinations are inevitable parts of the optoelectronic devices. Several works on the analysis of SPP propagation in these shapes have been reported to our knowledge. G. Veronis et al. [28] showed that bends and splitters can be designed over a wide frequency range without much loss by keeping centre layer thickness small compared to wavelength. H. Gao et al.[29] investigated the propagation and combination of SPP in Y-shaped channels. B. Wang et al.[30] analyzed two structures which consist of splitting and recombination. In the past years, several plasmonic couplers have been proposed by different researchers. G. Veronis et. Al.[31] proposed a coupler with multi-section tapers. P. Ginzburg et al.[32] reported a λ/4 coupler to couple optical modes from a 0.5m to 50nm wide plasmonic waveguide. D. Pile et al.[33] presented an adiabatic and a non-adiabatic tapered plasmonic coupler. R. Washleh et al.[34] reported an analysis on nanoplasmonic air-slot coupler and its fabrication steps.

1.3: Thesis Objective

In our thesis we mainly focused in designing a plasmonic waveguide which has the characteristics of a high pass filter. In order to achieve that we had go through a number of learning steps. So basically the objectives are

- To develop a simulation model based on the FDTD method that is capable of simulating the device.
- To obtain the output transmittance of the designed structure so as to compare the results with a high pass filter and thus validate the authenticity of the waveguide.
- Finally summarize the conclusions from the results obtained and discuss the future potentials of the accomplished work.

1.4: Thesis Organization

Our approach has been organized in the following way:-

- In chapter 2 we described the basic theory of SPP propagation along with the introduction to fundamental knowledge and necessary mathematical formulations.
- Material modelling is an indispensable part in our thesis work. So in chapter 3 we described the widely used models for material modelling.
- In our entire simulations we used FDTD method. In chapter 4 an introduction to FDTD fundamentals for 1D and 2D are given. Along with the various aspects of FDTD, chapter 4 also introduces the absorbing boundary conditions.
- In chapter 5 modified Debey model, Lorentz model is discussed and also a developed simulation model is established.

- In chapter 6 the waveguide structure design and the variation of the corrugation parameters is discussed.
- In chapter 7 the performance of the waveguides and the transmission spectra are analysed.

Chapter 2

Propagation of SPP

2.1: Introduction

Surface Plasmon Polaritons (SPPs), are infrared or visible-frequencyelectro-magnetic waves, which travel along a metal-dielectric or metal-air interface. The term "surface plasmon polariton" explains that the wave involves both charge motion in the metal ("surface plasmon") and electromagnetic waves in the air or dielectric ("polariton").

Electromagnetic wave propagation is obtained from the solution of Maxwell's equations in each medium, and the asso-ciated boundary conditions. Maxwell's equations of macroscopic electromagnetism can be written as follows:

From Gauss's Law for the electric field

$$\nabla . \mathrm{D} = \rho_{\mathrm{ext}} \tag{2.1}$$

From Gauss's Law for the magnetic field

$$\nabla . \mathrm{B} = 0 \tag{2.2}$$

From Faraday's Law

$$\nabla \times \mathrm{E} = -\frac{\partial \mathrm{B}}{\partial \mathrm{t}} \tag{2.3}$$

From Ampere's Law

$$\nabla \times \mathrm{H} = \mathrm{J}_{\mathrm{ext}} + \frac{\partial \mathrm{D}}{\partial \mathrm{t}} \tag{2.4}$$

Here,

E is the electric field vector in volt per meter

D is the electric flux density vector in coulombs per square meter

H is the magnetic field vector in amperes per meter

B is the magnetic flux density vector in webbers per square meter

ρ_{ext} is the charge density

J_{ext} is the current density

The four macroscopic fields can be also linked further via the polarization P and magnetization M by

$$\mathrm{D} = \varepsilon_0 \mathrm{E} + \mathrm{P} \tag{2.5}$$

$$\mathrm{H} = \frac{1}{\mu_0} \mathrm{B} - \mathrm{M} \tag{2.6}$$

Now this equations can be simplified for linear, isotropic, nonmagnetic media as

$$\mathrm{D} = \varepsilon_0 \varepsilon_r \mathrm{E} \tag{2.7}$$

$$\mathrm{B} = \mu_0 \mu_r \mathrm{H} \tag{2.8}$$

where,

ε_0 is electric permittivity of vacuum in Farad per meter

$\mu_0$is the magnetic permeability of vacuum in Henry per meter

$\varepsilon_r$is the relative permittivity

$\mu_r$is the relative permeability

2.2: Electromagnetic Wave Equations

The EM wave equation which describes the field amplitude in time and space can be derived from Maxwell's equations. The wave equation can be derived by taking curl of Faraday's law

$$\nabla \times \nabla \times \mathrm{E} = -\frac{\partial \mathrm{B}}{\partial \mathrm{t}} \tag{2.09}$$

or,

$$\nabla \times \nabla \times \mathrm{E} = \nabla \times (-\mu \frac{\partial \mathrm{H}}{\partial \mathrm{t}}) \tag{2.10}$$

with the identities $\nabla \times \nabla \times E = \nabla(\nabla.E) - \nabla^2 E$ and $\nabla \times H = \varepsilon \frac{\partial E}{\partial t}$ we can simplify the above equation as

$$\nabla(\nabla.\mathrm{E}) - \nabla^2 \mathrm{E} = -\mu\varepsilon \frac{\partial^2 \mathrm{y}}{\partial \mathrm{t}^2} \tag{2.11}$$

From Gauss's law we can conclude that the divergence of E in a constant permittivity over space is zero. i,e $\nabla.E = 0$

Therefore, the final wave equation for electric field will be

$$\nabla^2 \mathrm{E} - \mu\varepsilon \frac{\partial^2 \mathrm{E}}{\partial \mathrm{t}^2} = 0 \tag{2.12}$$

Similarly the wave equation for magnetic field can be derived as

$$\nabla^2 \mathrm{H} - \mu\varepsilon \frac{\partial^2 \mathrm{H}}{\partial \mathrm{t}^2} = 0 \tag{2.13}$$

So, the general form of wave equation can be written as

$$\nabla^2 \mathrm{U} - \frac{1}{\upsilon_\mathrm{p}^2} \left(\frac{\partial^2 \mathrm{H}}{\partial \mathrm{t}^2}\right) = 0 \tag{2.14}$$

If the variation of the dielectric profile " is negligible over distance, then we can write

$$\nabla^2 \mathrm{E} - \frac{\varepsilon}{\mathrm{C}^2} \frac{\partial^2 \mathrm{E}}{\partial \mathrm{t}^2} = 0 \tag{2.15}$$

Where $C = \frac{1}{\sqrt{\mu_0 \varepsilon_0}}$ velocity of light

The solution of wave equation is a harmonic function in time and space. Now if we assume this as a harmonic time dependence of the electric field,

$$E(r,t) = E(r)e^{-j\omega t} \tag{2.16}$$

Therefore we get the Helmholtz equation

$$\nabla^2 E + K_0^2 \varepsilon E = 0 \tag{2.17}$$

where the vector of propagation $K_0 = \frac{\omega}{C}$, in free space

For simplicity let us assume the propagation of wave is along the x-direction of the Cartesian co-ordinate system and no spatial variation in y-direction. So we can write

$$E(x,y,z) = E(z)e^{j\beta z} \tag{2.18}$$

Where $\beta = K_x$ which is call the propagation constant

Now inserting the value of E the wave equation will be

$$\frac{\partial^2 E(z)}{\partial z^2} + (K_0^2 \varepsilon - \beta^2)E = 0 \tag{2.19}$$

Similarly we can derive the equation for the magnetic field H. The field E and H can be decomposed in cartesian co-ordinate system as

$$E = E_x.\vec{a}_x + E_y.\vec{a}_y + E_z.\vec{a}_z \tag{2.20}$$

$$H = H_x.\vec{a}_x + H_y.\vec{a}_y + H_z.\vec{a}_z \tag{2.21}$$

For Harmonic time dependence $\frac{\partial}{\partial t} = -j\omega$ and by solving the Ampere's law and Faraday's law, we get

$$\frac{\partial E_z}{\partial y} - \frac{\partial E_y}{\partial z} = j\omega\mu_0 H_x \tag{2.22}$$

$$\frac{\partial E_x}{\partial z} - \frac{\partial E_z}{\partial x} = j\omega\mu_0 H_y \quad (2.23)$$

$$\frac{\partial E_y}{\partial x} - \frac{\partial E_x}{\partial y} = j\omega\mu_0 H_z \quad (2.24)$$

$$\frac{\partial Hz}{\partial y} - \frac{\partial H_y}{\partial z} = j\omega\varepsilon_0 \varepsilon E_x \quad (2.25)$$

$$\frac{\partial Hx}{\partial z} - \frac{\partial H_z}{\partial x} = j\omega\varepsilon_0 \varepsilon E_y \quad (2.26)$$

$$\frac{\partial Hy}{\partial x} - \frac{\partial H_x}{\partial y} = j\omega\varepsilon_0 \varepsilon E_z \quad (2.27)$$

As the propagation is in x-direction in the form of $e^{j\beta x}$ which follows $\frac{\partial}{\partial x} = -j\beta$.

The homogeneity in y- direction make $\frac{\partial}{\partial y} = 0$. So the equation will be simplified as

$$-\frac{\partial E_y}{\partial z} = j\omega\mu_0 H_x \quad (2.28)$$

$$\frac{\partial E_x}{\partial z} - j\beta E_z = j\omega\mu_0 H_y \quad (2.29)$$

$$j\beta E_y = j\omega\mu_0 H_z \quad (2.30)$$

$$\frac{\partial H_y}{\partial z} = j\omega\varepsilon_0 \varepsilon E_x \quad (2.31)$$

$$\frac{\partial Hx}{\partial z} - j\beta H_z = j\omega\varepsilon_0 \varepsilon E_y \quad (2.32)$$

$$j\beta H_y = j\omega\varepsilon_0 \varepsilon E_z \quad (2.33)$$

The solution of the above equation can be characterized by two sets of solution with the polarized characteristics which are, Transverse Magnetic (TM) modes and Transverse Electric (TE) modes. The equations belong to TM modes are

$$E_x = -j\frac{1}{\omega\varepsilon_0\,\varepsilon}\frac{\partial H_y}{\partial z} \tag{2.34}$$

$$E_z = -\beta\frac{1}{\omega\varepsilon_0\,\varepsilon}H_y \tag{2.35}$$

Therefore, the wave equation for TM Polarized wave will be

$$\frac{\partial^2 H_y}{\partial z^2} + (K_0^2\varepsilon - \beta^2)H_y = 0 \tag{2.36}$$

Similarly the TE polarized equations will be

$$H_x = j\frac{1}{\omega\mu_0}\frac{\partial E_y}{\partial z} \tag{2.37}$$

$$H_z = \beta\frac{1}{\omega\mu_0}E_y \tag{2.37}$$

And the corresponding TE wave equation will be

$$\frac{\partial^2 E_y}{\partial z^2} + (K_0^2\varepsilon - \beta^2)E_y = 0 \tag{2.38}$$

2.3: Single Interface SPP

The simplest configuration of SPP propagation is at single interface, that is in between dielectric, having the positive dielectric constant ε_2 and metal, having the negative dielectric constant ε_1. For metal the bulk plasmon frquency will be ω_p and the amplitude decays perpendicular to the z− direction.

For the TM solutions in both spaces: metal and dielectric will be for z > 0

$$H_z(z) = A_2 e^{j\beta x} e^{-k_2 z} \tag{2.40}$$

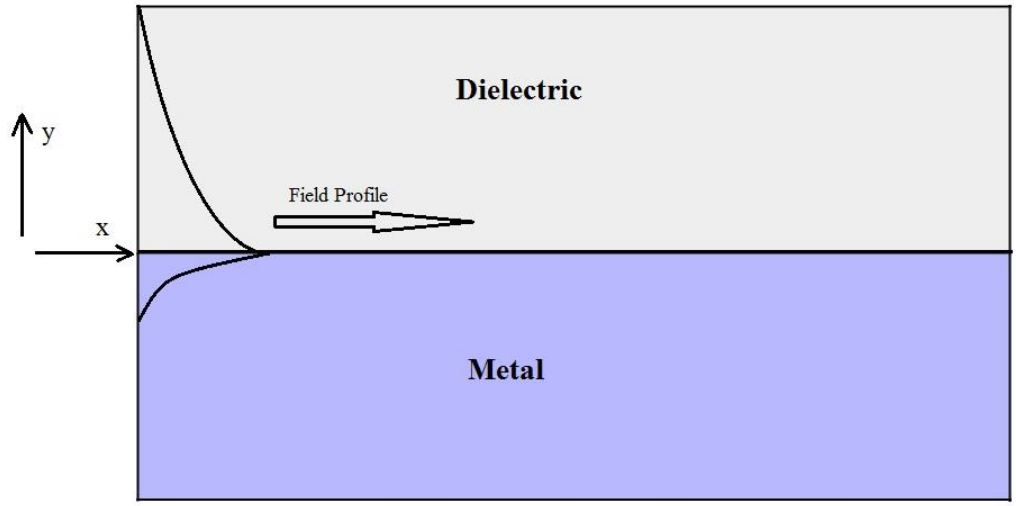

Fig 2.1: SPP at the Single interface.

$$E_x(z) = jA_2 \frac{1}{\omega\varepsilon_0 \varepsilon_2} k_2 e^{j\beta x} e^{-k_2 z} \tag{2.41}$$

$$E_z(z) = -A_1 \frac{\beta}{\omega\varepsilon_0 \varepsilon_2} e^{j\beta x} e^{-k_2 z} \tag{2.42}$$

And for z < 0

$$H_y(z) = A_1 e^{j\beta x} e^{k_1 z} \tag{2.43}$$

$$E_x(z) = -jA_1 \frac{1}{\omega\varepsilon_0 \varepsilon_1} k_1 e^{j\beta x} e^{k_1 z} \tag{2.44}$$

$$E_x(z) = -A_1 \frac{\beta}{\omega\varepsilon_0 \varepsilon_1} e^{j\beta x} e^{-k_1 z} \tag{2.45}$$

The continuity of H_y and $\varepsilon_i E_z$ at the metal dielectric interface gives $A_1 = A_2$ and

$$\frac{k_2}{k_1} = -\frac{\varepsilon_2}{\varepsilon_1} \tag{2.46}$$

The surface wave exists at the metal dielectric interface with opposite sign of their real dielectric permittivity. So, we can write

$$k_1^2 \varepsilon = \beta^2 - k_0^2 \varepsilon_1 \tag{2.47}$$

$$k_2^2\varepsilon = \beta^2 - k_0^2\varepsilon_2 \tag{2.48}$$

The dispersion relation of SPPs propagation can be found as

$$\beta = k_0\sqrt{\frac{\varepsilon_1\varepsilon_2}{\varepsilon_1+\varepsilon_2}} \tag{2.49}$$

The TE surface modes can be expressed as

$$E_y(z) = A_2 e^{j\beta x}e^{-k_2 z} \tag{2.50}$$

$$H_x(z) = -jA_2\frac{\beta}{\omega\mu_0}k_2 e^{j\beta x}e^{-k_2 z} \tag{2.51}$$

$$H_z(z) = -A_2\frac{\beta}{\omega\mu_0}k_2 e^{j\beta x}e^{-k_2 z} \tag{2.52}$$

for z > 0, and

$$E_y(z) = A_1 e^{j\beta x}e^{-k_1 z} \tag{2.53}$$

$$H_x(z) = jA_1\frac{\beta}{\omega\varepsilon_0\,\varepsilon_1}k_1 e^{j\beta x}e^{k_1 z} \tag{2.54}$$

$$H_z(z) = A_1\frac{\beta}{\omega\varepsilon_0\,\varepsilon_1}k_2 e^{j\beta x}e^{k_1 z} \tag{2.55}$$

for z < 0. The continuity of E_y and H_x requires

$$A_1 (k_1 + k_2) = 0 \tag{2.56}$$

The surface requires that the real part of k_1 and k_2 should be greater than zero for confinement. This will be satisfied if $A_1 = A_2 = 0$. Therefore no surface modes for the TE polarization. SPP only exist for TM mode polarization.

2.4: Double Interface SPP

Two mostly used double interface configurations of SPP waveguides are: Metal-Dielectric-Metal(MDM) and Dielectric-Metal-Dielectric (DMD). In these cases SPPs are formed on both interfaces. When the distance is shorter than decay distance, it forms coupled mode of SPP. This coupled mode of propagation can also be sub-divided into even and odd modes, as shown in the figure

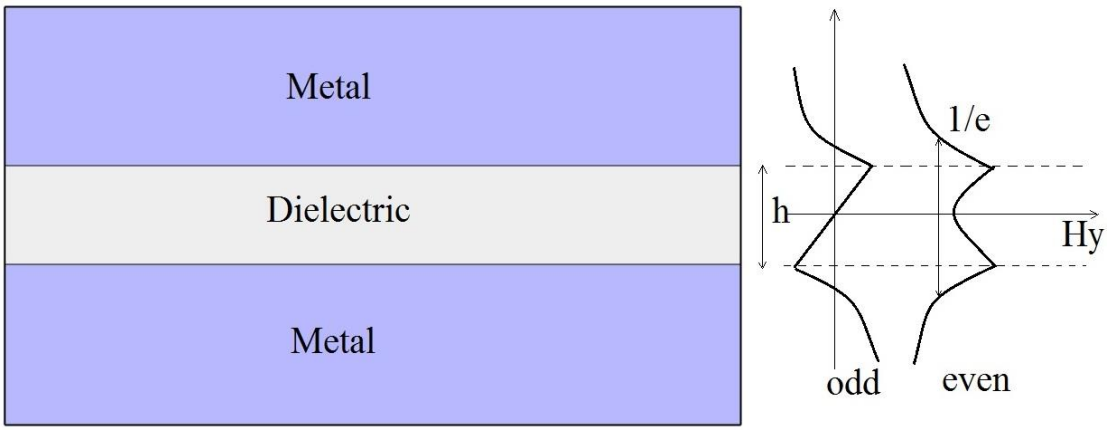

Fig 2.2: SPP at the double interface.

Chapter 3

Material Modelling

3.1: Introduction

At low frequencies or for long wavelengths metals act as perfect conductors. Since it has zero field, they do not show any dispersive behavior. But at higher frequen-cies such as optical range metals behave as dispersive materials which means that there exists field inside metal. And for the frequencies higher than optical range metals act as dielectrics. Properties of SPPs depend highly on the material re-sponse to light. In this chapter we will be studying about the material supporting SPP, descriptions and derivations of different models for describing the behavior of metal in the presence of light.

Now in presence of an external oscillating electromagnetic field, three vectors can determine the behavior of any material. Such as: D (electrical flux density), E (electric field intensity) and P (polarization density). In frequency domain the corresponding equation will be

$$D(\omega) = \varepsilon(\omega)E(\omega) \tag{3.1}$$

$$P(\omega) = \varepsilon_0\chi(\omega)E(\omega) \tag{3.2}$$

$$D(\omega) = \varepsilon_0 E(\omega) + P(\omega) \tag{3.3}$$

Combining this two equations we get

$$D(\omega) = \varepsilon_0 E(\omega)(1 + \chi(\omega)) \tag{3.4}$$

Where χ is the electric susceptibility which measures how easily it is polarized in response to an applied electric field, and it is a dimensionless quantity.

Finally the relation between the the permittivity and susceptibility is

$$\varepsilon(\omega) = \varepsilon_0(1 + \chi(\omega)) \tag{3.5}$$

So the relative permittivity will be

$$\varepsilon_r(\omega) = 1 + \chi(\omega) \tag{3.6}$$

For linear isotropic materials such as glass this above values become simple. But for a dispersive material, the frequency dependent permittivity and susceptibility should be modeled perfectly for getting the perfect response of the material for certain electromagnetic excitation. Some widely used material models are Drude model, Lorentz model, Debye model and Lorentz-Drude model.

3.2: Different Material Models

3.2.1: Drude Model

The Drude model of electrical conductionwas proposed in 1900 by Paul Drude to explain the transport properties of electrons in materials (especially metals). The model, which is an application of kinetic theory. The Drude model considers the metal to be formed of a mass of positively charged ions from which a number of "free electrons" were detached. These may be thought to have become delocalized when the valence levels of the atom came in contact with the potential of the other atoms. The electrons in a metal are subjected to two forces, such as

1. Driving force F_d
2. Damping force F_g

The driving force and the damping force can be expressed as

$$F_d = qE = -eE \tag{3.6}$$

$$F_g = -\Gamma\upsilon \tag{3.7}$$

As the two forces are opposite to each other, the resultant force will be

$$F = F_d - F_g \tag{3.8}$$

From Newton's first law of motion we can write

$$mr'' = -eE + \Gamma r' \tag{3.9}$$

where,

m is the mass of an electron

Γ is the damping constant in Newton second per meter

r is the displacement in meter.

v is the velocity of the electron .

q is the electrons charge.

The prime indicates differentiation order with respect to time

For time harmonic electric field and time harmonic displacement the equation will be

$$E(t) = E_0 e^{-j\omega t} \Leftrightarrow E(\omega) \tag{3.10}$$

$$r(t) = R_0 e^{-j\omega t} \Leftrightarrow R(\omega) \tag{3.11}$$

From equaion 3.10 the frequency domain form will be

$$mR''(\omega) - \Gamma mR'(\omega) + eE(\omega) = 0 \tag{3.12}$$

The derivatives of frequency domain will give

$$-m\omega^2 R''(\omega) + j\omega\Gamma mR'(\omega) + eE(\omega) = 0 \tag{3.13}$$

Simplifying the above equation, the displacement R will give

$$R(\omega) = \frac{-e}{m(j\Gamma\omega - \omega^2)} E(\omega) \tag{3.14}$$

The polarization for n number of electrons will be

$$P(\omega) = -neR(\omega) \tag{3.15}$$

Or,

$$P(\omega) = \frac{e^2 n}{m(j\Gamma\omega - \omega^2)} E(\omega) \tag{3.16}$$

An expression for the susceptibility can also be obtained from the above equation and that will be

$$\frac{P(\omega)}{\varepsilon_0 E(\omega)} = \frac{e^2 n}{\varepsilon_0 m(j\Gamma\omega - \omega^2)} = \chi(\omega) \tag{3.17}$$

Now substituting this value in equation 3.6 we get

$$\varepsilon_r(\omega) = 1 + \frac{e^2 n}{\varepsilon_0 m(j\Gamma\omega - \omega^2)} \tag{3.18}$$

if we consider ω_p as the plasma frequency that will provide

$$\omega_p^2 = \frac{e^2 n}{\varepsilon_0 m} \tag{3.19}$$

So, the frequency dependent flux density will be

$$D(\omega) = \varepsilon_0 (1 + \frac{\omega_p^2}{(j\Gamma\omega - \omega^2)}) E(\omega) \tag{3.20}$$

For low frequency, the term $\Gamma\omega \ll 1$ therefore, the dispersive relation can be reduced to

$$D(\omega) = \varepsilon_0(1 - \frac{\omega_p^2}{(\omega^2)})E(\omega) \quad (3.21)$$

3.2.2: Lorentz Model

The Lorentz model gives a simpler picture of the atom. The model is a very useful tool to visualize atom-field interaction. In this model, Lorentz modeled an atom as a mass (nucleus) connected to another smaller mass (electron). However, electrons in the Lorentz model do not move freely inside the metal instead, they are bound to atoms. So, there is a restoring force acting between them which can be denoted by F_r

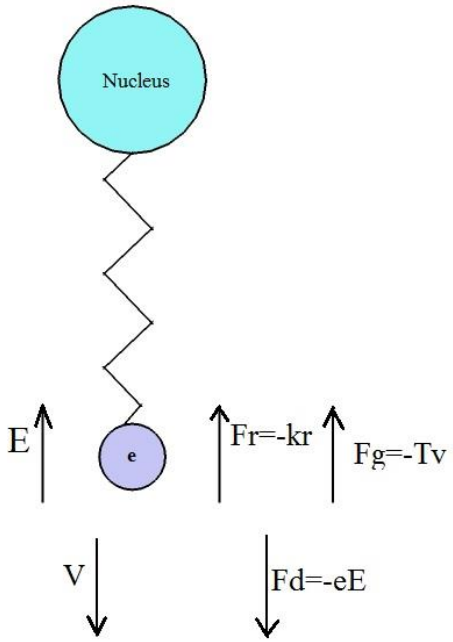

Fig 3.1: Lorentz model

The restoring force can be written as

$$F_r = -kr \quad (3.22)$$

where k is the spring constant in Newtons per meter.

Similarly from the law of motion we can say that

$$mr'' + \Gamma mr'(\omega) + mkr + eE = 0 \quad (3.23)$$

In frequency domain the above equation will be

$$R(\omega)(m\omega_0^2 + j\omega\Gamma m - m\omega^2 - eE(\omega) = 0 \tag{3.24}$$

Considering the natural frequency $\omega_0 = \sqrt{\frac{k}{m}}$ we get

$$R(\omega) = \frac{-e}{m(\omega_0^2 + j\omega\Gamma - \omega^2)} E(\omega) \tag{3.25}$$

Therefore the susceptibility can be found as

$$\frac{P(\omega)}{\varepsilon_0 E(\omega)} = \frac{e^2 n}{\varepsilon_0 m(\omega_0^2 + j\omega\Gamma - \omega^2)} = \chi(\omega) \tag{3.26}$$

So from the equation 3.4 the expression for D can be expressed in frequency domain as

$$D(\omega) = \varepsilon_0(1 + \frac{\omega_p^2}{\omega_0^2 + j\omega\Gamma - \omega^2})E(\omega) \tag{3.27}$$

3.2.3: Lorentz Drude Model

In the Lorentz-Drude (LD) model, which is the most general form when an EM field is applied to a metal, the electrons of two types oscillate inside the metal, and they contribute to the permittivity. The free electrons contribute a permittivity of the Drude model, and the bound electrons contribute a permittivity of the Lorentz model. The permittivity in the LD model is given by

$$\varepsilon = \varepsilon_{free} + \varepsilon_{bound} \tag{3.29}$$

Where

$$\varepsilon_{free} = 1 + \frac{\omega_p}{(j\Gamma\omega - \omega^2)} \tag{3.30}$$

$$\varepsilon_{bound} = \frac{\omega_p}{\omega_0 + j\omega\Gamma - \omega^2} \quad (3.31)$$

Therefore combining both the model together the electric field density D in fre-quency domain will be

$$D(\omega) = \varepsilon_0\left(1 + \frac{\omega_p}{j\Gamma\omega - \omega^2} + \frac{\omega_p^2}{\omega_0^2 + j\omega\Gamma - \omega^2}\right)E(\omega) \quad (3.32)$$

The above relation is known as the Lorentz-Drude model.

3.2.4: Debye Model

The Debye model was first developed by Peter Debye in the year 1912. According to the Debye model,materials are made of electric dipoles, so that, when an electric field is applied, these dipoles follow the behavior of the applied field with some relaxation time. If the electric field is oscillating at a slow frequency, then the polarization will be strong. On the other hand, a fast oscillating field means low polarization. From another point of view, materials with long relaxation times have low polarization or no polarization at all, and materials with short relaxation times have strong polarization. Metals are known to have very short relaxation times. Thus, polarization in metals is strong. If a DC electric field is applied to a dielectric, the polarization takes some time to follow the electric field. At steady state, it will be

$$P(t) = P_\infty\left(1 - e^{-t/\tau}\right) \quad (3.33)$$

where P (t) is the instantaneous polarization

P_∞ is the polarization in the steady state is the time constant.

The derivative of the above equation will be

$$\frac{dP(t)}{dt} = \frac{1}{\tau} P_{\infty} e^{-t/\tau} \quad (3.34)$$

Now combining both the equations we get

$$P(t) = P_{\infty} - \tau \frac{dP(t)}{dt} \quad (3.35)$$

As $P_{\infty} = \varepsilon_0 (\varepsilon - 1) E(t)$ so the equation will be reduced to

$$P(t) = \varepsilon_0 (\varepsilon - 1) E(t) - \tau \frac{dP(t)}{dt} \quad (3.36)$$

or,

$$\varepsilon_0 (\varepsilon - 1) E(t) = P(t) + \tau \frac{dP(t)}{dt} \quad (3.37)$$

In frequency domain the equation will be

$$\varepsilon_0 (\varepsilon - 1) E(\omega) = P(\varepsilon) + j\omega\tau P(\omega) \quad (3.38)$$

Or,

$$P(\omega) = \frac{\varepsilon_0 (\varepsilon - 1)}{1 + j\omega\tau} E(\omega) \quad (3.39)$$

The susceptibility can be expressed as

$$\frac{(\varepsilon - 1)}{1 + j\omega\tau} = \frac{P(\omega)}{\varepsilon_0 E(\omega)} = \chi(\omega) \quad (3.40)$$

The relative permittivity will be

$$\varepsilon_0(\omega) = \frac{(\varepsilon - 1)}{1 + j\omega\tau} + 1 = 1 + \chi(\omega) \quad (3.41)$$

For the permittivity function to fit in the range from 0 frequency to infinity frequency, the boundary conditions are $\varepsilon_r(0) = \varepsilon_s$ (0) and $\varepsilon_r(\infty) = \varepsilon_\infty$ (0)

So,

$$\varepsilon(\omega) = \varepsilon_\infty + \frac{(\varepsilon_s - \varepsilon_\infty)}{1 + j\omega\tau} \quad (3.42)$$

To take into account the material losses that SPPs encounter, another term is added with the permittivity of metal. So the above equation can be expanded to

$$\varepsilon(\omega) = \varepsilon_\infty + \frac{(\varepsilon_s - \varepsilon_\infty)}{1+j\omega\tau} - j\frac{\sigma}{\omega\varepsilon_0} \quad (3.43)$$

In real and imaginary term the Debay model is

$$\varepsilon_r(\omega) = \varepsilon'(\omega) - j\varepsilon''(\omega) \quad (3.44)$$

Where-

$$\varepsilon'(\omega) = \varepsilon_\infty + \frac{(\varepsilon_s - \varepsilon_\infty)\omega\tau}{1+j\omega^2 r^2} \quad (3.45)$$

$$\varepsilon''(\omega) = \varepsilon_\infty + \frac{(\varepsilon_s - \varepsilon_\infty)\omega\tau}{1+j\omega^2 r^2} + \frac{\sigma}{\omega\varepsilon_0} \quad (3.46)$$

3.3: Material Dispersion

Dispersion can be defined as the variation of the propagating waves wavelength with frequency. It is also sometimes defined as the variation of propagating waves wave number k =$\frac{2\pi}{\lambda}$with angular frequency ω = 2πf. So the one dimensional wave equation will be

$$\frac{\partial^2 u}{\partial t^2} = \upsilon^2 \frac{\partial^2 u}{\partial x^2} \quad (3.47)$$

Where,

$$\upsilon^2 = \frac{1}{\varepsilon\mu}$$

The solution of the above wave equation can be written in phasor form as

$$u(x,t) = e^{j(\omega t - kx)} \quad (3.48)$$

Now putting this value in the wave equation we get

$$(j\omega)^2 e^{j(\omega t - kx)} = \upsilon^2(-jk)^2 e^{j(\omega t - kx)} \quad (3.49)$$

Finally from this equation we get

$$k = \pm \frac{\omega}{\upsilon} \tag{3.50}$$

The + sign is for -x directed wave propagation and - sign is for +x directed wave propagation. The magnetic flux density and electric flux density for dispersive medium are-

$$D(\omega) = \varepsilon(\omega)E \tag{3.51}$$

$$B(\omega) = \mu(\omega)H \tag{3.52}$$

Here both $\varepsilon(\omega)$ and $\mu(\omega)$ are frequency dependent functions.

Chapter 4

Finite Difference Time Domain Method

4.1: Yee Algorithm

The Yee algorithm is defined as the algorithm used in FDTD simulations. To calculate electromagnetic field propagation we want to solve Maxwell's equation that link electric and magnetic field components and its time and space evolution. The basic idea being FDTD technique is a successive update of electric and magnetic field components that are specially placed in the computational volume. The benefit of this scheme is that we can easily draw a electric field loop around a concrete component of the magnetic field and vice versa. This simplifies the implementation of rotations in the Maxwell equations significantly.

Every computation step has two parts:

1 Magnetic field components are updated from electric field components from the previous step.

2 Electric field components are updated from magnetic field components.

For update of any component we need only surrounding field values which makes the method suitable for parallelization.

FDTD is a time domain method, so we are always calculating a evolution of electromagnetic field in time.

The method begins with two of Maxwell's equations:

$$\mathrm{D}\frac{\partial \vec{\mathrm{H}}}{\partial \mathrm{t}} = -\frac{1}{\mu}\nabla \times \vec{\mathrm{E}} \tag{4.1}$$

$$\mathrm{D}\frac{\partial \vec{\mathrm{E}}}{\partial \mathrm{t}} = \frac{1}{\varepsilon}\nabla \times \vec{\mathrm{H}} \tag{4.2}$$

The electric and magnetic fields are three dimensional vectors. Each equation can be

converted into three coupled scalar first order differential equations. The derivatives are both in space and time. The curl operations of equations 4.1 and equation 4.2 yields the following six equations in Cartesian coordinates

$$\frac{\partial E_z}{\partial y} - \frac{\partial E_y}{\partial z} = \mu \frac{\partial H_x}{\partial t} \tag{4.3}$$

$$\frac{\partial E_x}{\partial z} - \frac{\partial E_z}{\partial x} = \mu \frac{\partial H_z}{\partial t} \tag{4.4}$$

$$\frac{\partial E_y}{\partial x} - \frac{\partial E_x}{\partial y} = \mu \frac{\partial H_z}{\partial t} \tag{4.5}$$

$$\frac{\partial Hz}{\partial y} - \frac{\partial H_y}{\partial z} = \varepsilon \frac{\partial E_x}{\partial t} \tag{4.6}$$

$$\frac{\partial Hx}{\partial z} - \frac{\partial H_z}{\partial x} = \varepsilon \frac{\partial E_y}{\partial t} \tag{4.7}$$

$$\frac{\partial Hy}{\partial x} - \frac{\partial H_x}{\partial y} = \varepsilon \frac{\partial E_z}{\partial t} \tag{4.8}$$

Then the scalar differential equations are converted into difference equations. To do that, both space and time discretization is required. For space discretization, Yee visualized the field components arranged within a unit cell (voxel). The electric field components are stored on the corresponding cell edges, while the magnetic field components are stored on the corresponding face centers. The fields are located in a way where each E component is surrounded by four

H components and vice versa, which leads to a spatially coupled system of field circulations corresponding to the law of Faraday and Ampere. The figure 4.1 shows the Yee's spatial grid.

Considering a two dimensional TM (Transverse Magnetic) polarized field case,

$$\frac{\partial E_x}{\partial t} = \frac{1}{\varepsilon}\frac{\partial H_z}{\partial y} \tag{4.09}$$

$$\frac{\partial E_y}{\partial t} = \frac{1}{\varepsilon}\frac{\partial H_z}{\partial x} \tag{4.10}$$

$$\frac{\partial H_z}{\partial t} = \frac{1}{\mu}\left(\frac{\partial E_x}{\partial y} - \frac{\partial E_y}{\partial x}\right) \tag{4.11}$$

Central difference approximation is applied in each of the equations 4.9, 4.10 and 4.11 which finally conclude in a spatial scalar difference equations in 4.12, 4.13 and 4.14.

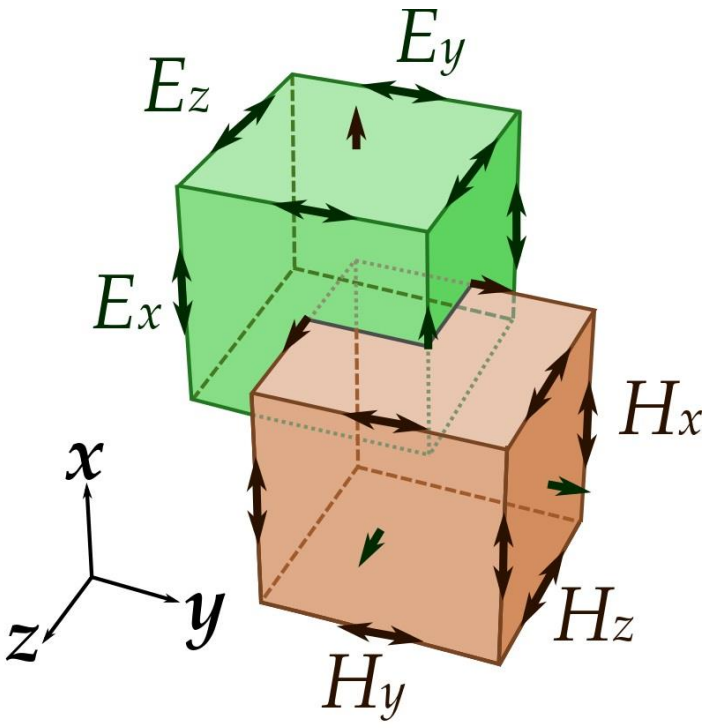

Fig 4.1: Yee's spatial grid.

$$\frac{\partial E_x}{\partial t} = \frac{1}{\varepsilon}\frac{H_z(i,j) - H_z(i,j-1)}{\Delta y} \tag{4.12}$$

$$\frac{\partial E_y}{\partial t} = \frac{1}{\varepsilon}\frac{H_z(i,j) - H_z(i-1,j)}{\Delta x} \tag{4.13}$$

$$\frac{\partial H_z}{\partial t} = \frac{1}{\mu}\left(\frac{E_x(i,j+1) - E_x(i,j)}{\Delta y} - \frac{E_y(i+1,j) - E_y(i-1,j)}{\Delta x}\right) \tag{4.14}$$

In order to consider the time derivatives, the time axis is to be considered as shown in

the figure. The Electric and Magnetic field are mapped half a step apart along the time axis. Again applying the central difference approximation the equations 4.12, 4.13 and 4.14 become:

$$\frac{E_x^{n+1}\left(i+\frac{1}{2},j\right) - E_x^{n}\left(i+\frac{1}{2},j\right)}{\Delta t} = \frac{1}{\varepsilon}\frac{H_z^{n+\frac{1}{2}}\left(i+\frac{1}{2},j\right) - H_z^{n+\frac{1}{2}}\left(i+\frac{1}{2},j-\frac{1}{2}\right)}{\Delta y}$$

$$\frac{E_y^{n+1}\left(i,j+\frac{1}{2}\right) - E_y^{n}\left(i,j+\frac{1}{2}\right)}{\Delta t} = -\frac{1}{\varepsilon}\frac{H_z^{n+\frac{1}{2}}\left(i+\frac{1}{2},j+\frac{1}{2}\right) - H_z^{n+\frac{1}{2}}\left(i-\frac{1}{2},j+\frac{1}{2}\right)}{\Delta y}$$

$$\frac{H_z^{n+\frac{1}{2}}\left(i+\frac{1}{2},j+\frac{1}{2}\right) - H_z^{n-\frac{1}{2}}\left(i+\frac{1}{2},j+\frac{1}{2}\right)}{\Delta t} = -\frac{1}{\mu}\left(\frac{E_x^{n+1}\left(i+\frac{1}{2},j+1\right) - E_x^{n}\left(i+\frac{1}{2},j\right)}{\Delta y} - \frac{E_y^{n}\left(i+1,j+\frac{1}{2}\right) - E_y^{n}\left(i,j+\frac{1}{2}\right)}{\Delta x}\right)$$

Each field component depends on the field of previous time step itself and the surrounding component in Yee's algorithm.

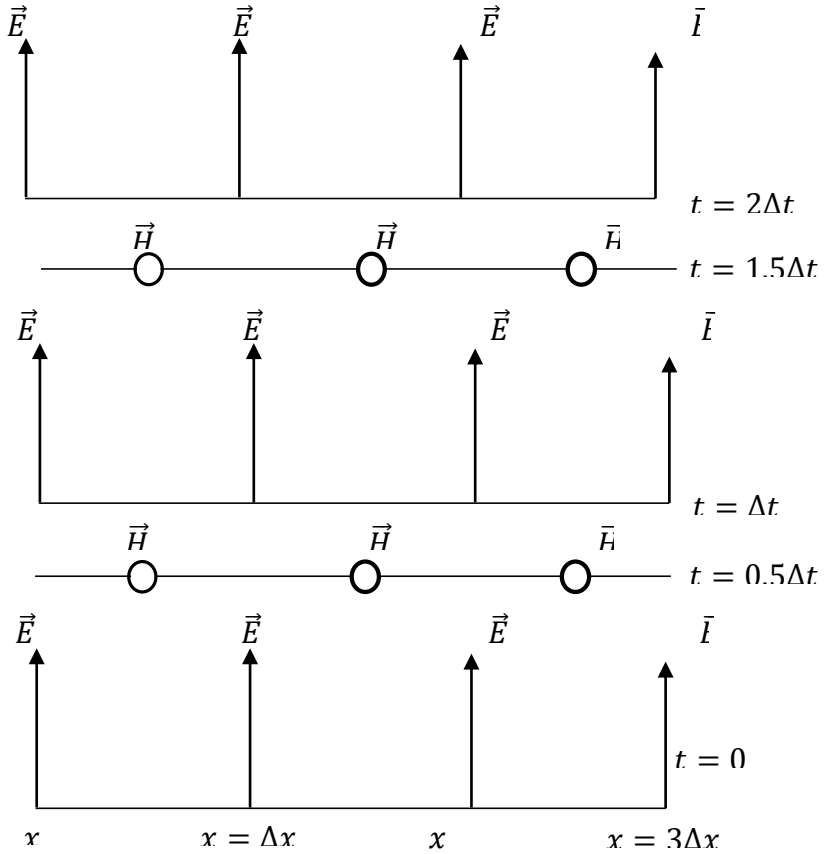

Fig 4.2: The temporal scheme of FDTD method.

Numerical stability of the Yee algorithm is required to be ensured. In an unstable algorithm the computed magnitude of electric and magnetic field components will gradually increase without limit with the progression of simulation. To guarantee numerical stability, the EM field's propagation should not be faster than the allowed limit which is imposed by the phase velocity within the material. This is done by limiting time step Δt using the Courant-Friedrichs-Lewy criterion for the general Yee FDTD grid as follows:

$$\Delta t \leq \left\{ \frac{1}{\upsilon \sqrt{\frac{1}{(\Delta x)^2}+\frac{1}{(\Delta y)^2}+\frac{1}{(\Delta z)^2}}} \right\} \tag{4.15}$$

where Δx, Δy and Δz indicate the spatial Cartesian grid increments.

4.2: Absorbing Boundary Condition

An absorbing boundary condition simulates infinite extent along a direction. This is accomplished by padding the side of the computational domain with artificial materials that absorbs incident electromagnetic fields. These artificial materials are convolution perfectly match layer(CPML), which currently offer the best absorption in the finite-time-difference-method.

4.3: Implementation of Material Dispersion in FDTD

If the permittivity and permeability of a material are functions of frequency then the material has the property of dispersion. So in order to accommodate dispersion property we need to have dispersive FDTD techniques. The FDTD based algorithms for the analysis of material dispersion can be divided into three types:

1) The auxiliary differential equation (ADE)
2) The Z-transform methods, and
3) Methods base on discrete convolution of the dispersion relation or the recursive convolution (RC) method [35].

4.3.1: The Auxiliary Differential Equation

Taflove introduced the auxiliary differential equation to the FDTD modeling in order to integrate the dispersion relation into the model. The dispersion relation is converted from frequency domain to time domain through Fourier transform in the basic step of the procedure. The Fourier transform results in a relationship between the new E field value and the previous E and D values, which can be added to the algorithm to update the E fields. The new algorithm with ADE becomes

$$\frac{\partial}{\partial t}H_z = -\frac{1}{\mu}\left(\frac{\partial E_x}{\partial y} - \frac{\partial E_y}{\partial x}\right) \quad (4.16)$$

$$\frac{\partial}{\partial t}D_x = \frac{\partial H_z}{\partial y} \quad (4.17)$$

In order to get the function relating D to E in a dispersive medium, we start with

$$D(\omega) = \varepsilon_0 \frac{\sigma}{j\omega} E(\omega) \quad (4.18)$$

Multiplying by $j\omega$

$$j\omega D(\omega) = \varepsilon_0 \sigma E(\omega) \quad (4.19)$$

Applying the Fourier transform in equation 4.19

$$\frac{d}{dt}D(t) = \varepsilon_0 \sigma E(t) \quad (4.20)$$

Discretizing equation 4.20 equation using forward difference method

$$\frac{D^n - D^{n-1}}{\Delta t} = \varepsilon_0 \sigma E(t) \quad (4.21)$$

Finally solving for E, we find the update equation

$$E^n = \frac{D^n - D^{n-1}}{\varepsilon_0 \sigma \Delta t} \quad (4.22)$$

4.3.2: Z-Transform Methods

The Z-transform is a faster method compared to ADE method. Sullivan used the Z-transform method for the first time in order to introduce the dispersion relation into the FDTD algorithm.

The Z-transform of the equation

$$D(\omega) = \varepsilon(\omega)E(\omega) \tag{4.23}$$

is -

$$D(z) = \varepsilon(z)\Delta t E(z) \tag{4.24}$$

where $\varepsilon(z)$ is the z-transform of $\varepsilon(\omega)$ and is the sampling period. As already done in ODE, let us consider the material dispersion as $\frac{\sigma}{j\omega}$, the relation between D and E is given by

$$D(\omega) = \frac{\sigma\varepsilon_0}{1-z^{-1}}\Delta t E(z) \tag{4.25}$$

Multiplying by $(1 - z^{-1})$, we find

$$D(z)(1 - z^{-1}) = \sigma\varepsilon_0 E(z) \tag{4.26}$$

or

$$D(z) - z^{-1}D(z) = \sigma\varepsilon_0 E(z) \tag{4.27}$$

Performing inverse z-transform

$$D^n - D^{n-1} = \sigma\varepsilon_0 \Delta t E^n \tag{4.28}$$

Finally, for solving E from equation 4.28, we find

$$E^{\mathrm{n}} = \frac{D^n - D^{n-1}}{\sigma \varepsilon_0 \Delta t} \tag{4.29}$$

Which is same as the final update equation derived by ADE method.

4.3.3: Piece-wise Linear Recursive Convolution Method

Luebbers et al. formulated the first frequency dispersive FDTD algorithm using the recursive convolution (RC) scheme. Later it became piecewise linear recursive convolution(PLRC) method [36]. Initially developed for Debye media [35], the ap-proach was later extended for the study of wave propagation in a Drude material [37], N-th order dispersive media [38], an anisotropic magneto-active plasma [39], ferrite material [40] and the bi-isotropic/chiral media [41] [42] [43].

The RC approach, typically being faster and having required fewer computer mem-ory resources than other approaches, is usually less accurate. But in case of mul-tiple pole mediums, it is easier to follow the RC approach.

In the initial derivation of PLRC method for a linear dispersive medium, the re-lation between electric flux density and electric field intensity is expressed as:

$$D(t) = \varepsilon_\infty \varepsilon_0 E(t) + \varepsilon_0 \int_0^t E(t-\tau)\chi(\tau)d\tau \tag{4.30}$$

which can be discretized as:

$$D^n = \varepsilon_\infty \varepsilon_0 E^n + \varepsilon_0 \int_0^{n\Delta t} E(n\Delta t - \tau)\chi(\tau)d\tau \tag{4.31}$$

The PRC method is further preceded from this basing discrete equation.

4.3.4: General Algorithm

The derivation of equations for multi-pole dispersion relation is more difficult compared to the single pole-pair dispersion relation. For example, for six-pole Lorentz-Drude dispersion the required derivation process is lengthy. Additionally, the memory required for computation is also vast. There are various methods proposed by researchers regarding this topic such as Taflove's matrix inversion method, Multi-term dispersion by Okoniewski, etc. However Alsunaidi and Al-Jabr proposed a general algorithm technique which solves various problems regard-ing previous methods. The major advantage of this technique is that it requires only one algorithm for anyt dispersion relation. The dispersive relation has the general form as

$$D(\omega) = \varepsilon(\omega)E(\omega) \tag{4.32}$$

which can be expressed in terms of summation of poles

$$D(\omega) = \varepsilon_\infty \, \varepsilon_0 E(\omega) + \sum_i^N P_i(\omega) \tag{4.33}$$

where N is the number of poles. Applying Fourier transform, this equation becomes

$$D^{n+1} = \varepsilon_\infty \, \varepsilon_0 E^{n+1} + \sum_i^N P_i^{n+1} \tag{4.34}$$

or

$$E^{n+1} = \frac{D^{n+1} - \sum_i^N P_i^{n+1}}{\varepsilon_\infty \, \varepsilon_0} \tag{4.35}$$

This term P_i can be any form of dispersion relation such as the Debye, the Drude or just the conductivity term. This the final solved equation for E.

Chapter 5

Extraction of Optical Material Parameters

The Modified Debye Model (MDM) parameters for silver metal is presented. A nonlinear optimization algorithm has been developed in order to extract the parameters for the metals. The extracted parameters have been used to determine the complex relative permittivity of the metals in optical and near-IR region of electromagnetic spectrum. The obtained results have been compared with the experimental values and an excellent agreement has been found.

5.1: Material Models

5.1.1: Modified Debye Model

5.1.1.1: Metals

The complex relative permittivity function of the modified Debye model is de-scribed by the following equation

$$\varepsilon_r(\omega) = \varepsilon_\infty + \frac{(\varepsilon_s - \varepsilon_\infty)}{1+j\omega\tau} - j\frac{\sigma}{\omega\varepsilon_0} \tag{5.1}$$

where, ε_∞ is the infinite frequency relative permittivity, ε_s is the zero frequency relative permittivity, ω is the angular frequency, σ is the conductivity and τ is the relaxation time.

If the model is represented in terms of its real and imaginary parts, then,

$$\varepsilon_r(\omega) = \varepsilon'(\omega) - j\varepsilon''(\omega) \tag{5.2}$$

where, the real part of the complex relative permittivity is,

$$\varepsilon'(\omega) = \varepsilon_\infty + \frac{(\varepsilon_s - \varepsilon_\infty)}{1 + (\omega\tau)^2}$$

and the imaginary part of the complex relative permittivity is,

$$\varepsilon''(\omega) = \frac{(\varepsilon_s - \varepsilon_\infty)}{1+(\omega\tau)^2} + \frac{\sigma}{\omega\varepsilon_0}$$

From equation 5.1, we can see that the modified Debye model can be described by four parameters which are ε_s, ε_∞,$\sigma$and τ. However, a relationship can be derived among these parameters by comparing equation 5.1 with the Drude model equation as,

$$\sigma = \frac{\varepsilon_0(\varepsilon_s - \varepsilon_\infty)}{\tau} \tag{5.3}$$

Now we actually have three parameters that need to be extracted and the other can be obtained from equation 5.3.

5.1.1.2: Di-electric Materials

The frequency dependent permittivity function of Modified Debye Model is given by

$$\varepsilon_r(\omega) = \varepsilon_\infty + \frac{(\varepsilon_s - \varepsilon_\infty)}{1+j\omega\tau} \tag{5.4}$$

where, ε_∞ is the infinite frequency relative permittivity, ε_s is the zero frequency relative permittivity, ω is the angular frequency and τ is the relaxation time.

From equation 5.4 we can see that modified Debye model for dielectric material can be described by three parameters which are ε_∞, ε_s and τ.These three parameters need to be optimized in order to model dielectric materials using MDM.

5.1.2: Lorentz Model

The frequency dependent complex permittivity function for single pole-pair Lorentz model is given by

$$\varepsilon_r(\omega) = \varepsilon_\infty + \frac{\omega_0^2\,(\varepsilon_s - \varepsilon_\infty)}{\omega_0^2 + j2\delta\omega - \omega^2} \tag{5.5}$$

where, ε_∞ is the infinite frequency relative permittivity, ε_s is the zero frequency relative permittivity, ω_0 is the frequency of the pole pair and δ is the damping frequency.

From equation 5.5, it can be observed that single pole-pair Lorentz model can be described by four parameters which are ε_∞, ε_s, ω_0 and δ. These four parameters are independent and need to be extracted.

5.1.3: Development of Simulation Model

The simulation model we have developed is based on the FDTD method. We have utilized the general auxiliary differential equation (ADE) based FDTD approach in order to incorporate the frequency dependent dispersion property of the constituent materials. This algorithm is useful for the simulation of materials with different dispersive properties. The perfectly matched layer has been integrated at all the boundaries in order to prevent back reflections.

Considering the material dispersion, the frequency-dependent electric flux density can be given by-

$$D(\omega) = \epsilon_o \epsilon_\infty E(\omega) + P(\omega). \tag{5.6}$$

The general Lorentz model for polarization (ω) is given by-

$$P(\omega) = \frac{a}{b+jc\omega-d\omega^2} E(\omega)\,, \tag{5.7}$$

By inverse Fourier transform, it can be written in time domain as-

$$bP(t) + cP'(t) + dP''(t) = aE(t). \tag{5.8}$$

Now, turning to FDTD scheme, above equation can be presented as-

$$P^{n+1} = C_1 P^n + C_2 P^{n-1} + C_3 E^n. \tag{5.9}$$

Where, $C_1 = \frac{4d-2b\Delta t^2}{2d+c\Delta t}$, $C_2 = \frac{-2d-c\Delta t}{2d+c\Delta t}$, and $C_3 = \frac{2a\Delta t^2}{2d+c\Delta t}$.

The values of C_1, C_2, C_3 depends on the material under consideration. Finally, equation of field intensity has the form-

$$E^{n+1} = \frac{D^{n+1}-\sum_{i=1}^{N} P_i^{n+1}}{\epsilon_o \epsilon_\infty} \tag{5.10}$$

Where N is the number of poles and D^{n+1} is the next value of electric flux density after one iteration in FDTD algorithm.

Chapter 6

Design of Plasmonic Waveguide Structure

6.1: Introduction

The propagation of Surface Plasmon Polariton can be implemented for the simulation of plasmonic waveguide. Plasmonic waveguide designs strive to maximize both the confinement and propagation length of surface plasmons within a plasmonic circuit. The construction of a practical and usable surface plasmon circuit is heavily dependent on a compromise between propagation and confinement. Maximizing both confinement and propagation length helps mitigate the drawbacks of choosing propagation length over confinement and vice versa. Multiple types of waveguides have been created in pursuit of a plasmonic circuit with strong confinement and sufficient propagation length, like insulator-metal-insulator (IMI), metal-insulator-metal (MIM) etc. The key performance parameters of an MIM(metal-insulator-metal) surface plasmonic waveguide having periodic corrugations has been investigated. The transmittance, taking into account a wide range of optical wavelength was demonstrated by rigorous numerical calculations against the variation of different structural aspects. The results indicate that a very satisfactory filtering characteristic can be achieved by this variation of the parameters The output of this investigation has the potential to develop ultra-compact photonic filters for higher integration

6.2: Waveguide Structures

6.2.1: Variation of Corrugation Height

We consider a thin corrugated air strip sandwiched between two layers of metal(silver) and the schematic diagrams of the MIM waveguide structures are

presented below with figures. The air strip is of 50 nm by which best propagation efficiency is attained. The corrugation width is 25 nm and a duty cycle of 50% is maintained throughout the structure.

In this figure we have varied the corrugation height(h). The height is increased from 0 nm to 55 nm. The step size is taken 5 nm.

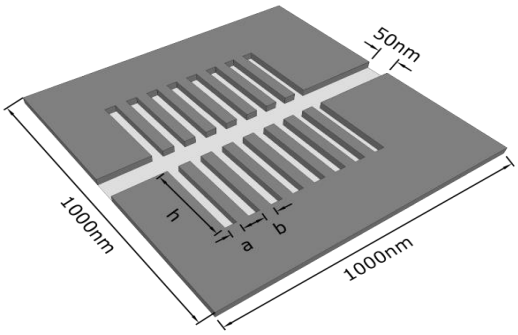

Fig 6.1: 3D view of the studied structure where the corrugation height(h) is increased from 0 nm to 55 nm with a step size of 5 nm.

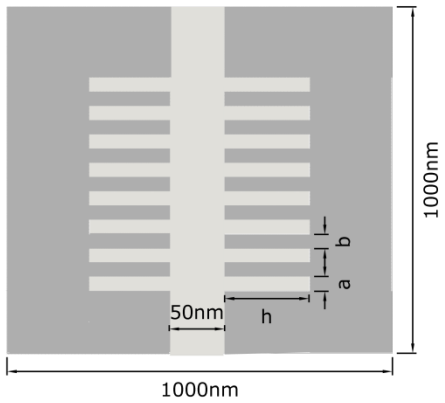

Fig 6.2: 2D view of the studied structure where the corrugation height(h) is increased from 0 nm to 55 nm with a step size of 5 nm.

6.2.2: Variation of Corrugation Depth

In this structure we have varied the corrugation depth(w). The variation starts from 0 nm and ends at 20 nm. Herein, the step size is also 5 nm. It is evident from the picture

that the silver layer is extended inside the air gap to constitute the depth of corrugation.

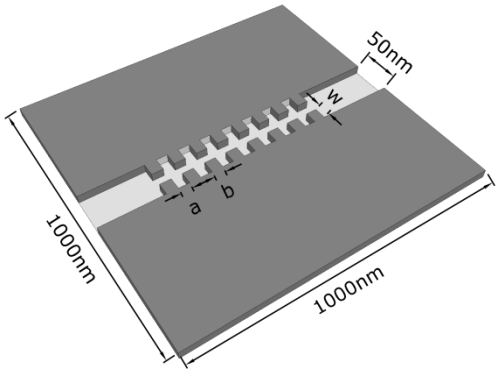

Fig 6.3: 3D view of the studied structure where the silver layer is extended inside the air gap and the depth(w) of the corrugation is varied from 0 nm to 20 nm with a step size of 5 nm.

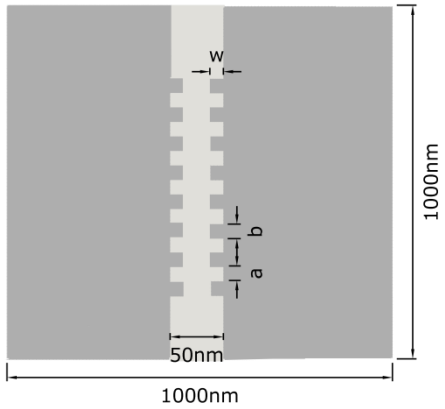

Fig 6.4: 2D view of the studied structure where the silver layer is extended inside the air gap and the depth(w) of the corrugation is varied from 0 nm to 20 nm with a step size of 5 nm.

6.2.3: Variation of Both Corrugation Height and Depth

n this figure the depth(w) is fixed at 15 nm and the corrugation height(h) is varied. It starts from 0 nm and ends at 55 nm with a step size of 5 nm.

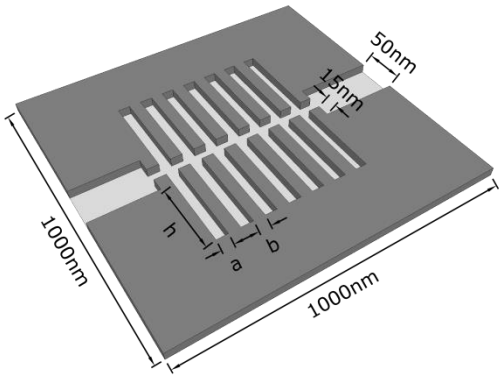

Fig6.5: 3D view of the studied structure where the corrugation depth(w) is fixed at 15 nm and the corrugation height(h) is varied from 0 nm to 55 nm with a step size of 5 nm.

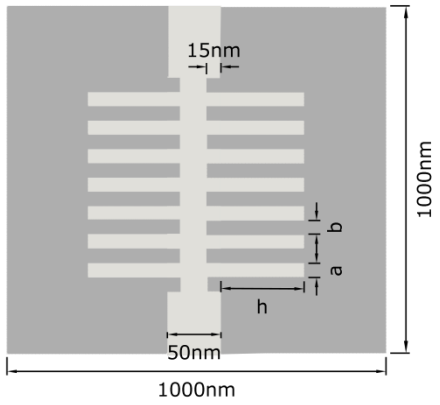

Fig 6.6: 2D view of the studied structure where the corrugation depth(w) is fixed at 15 nm and the corrugation height(h) is varied from 0 nm to 55 nm with a step size of 5 nm.

6.3: Simulation of Plasmonic Profile Propagation Through the Waveguides

For the simulation of the plasmon profile propagation, firstly plasmon profile is generated by the incidence of a photon pulse on the interface. Below are the E_x , E_y , Hz fields for the generated plasmon profile

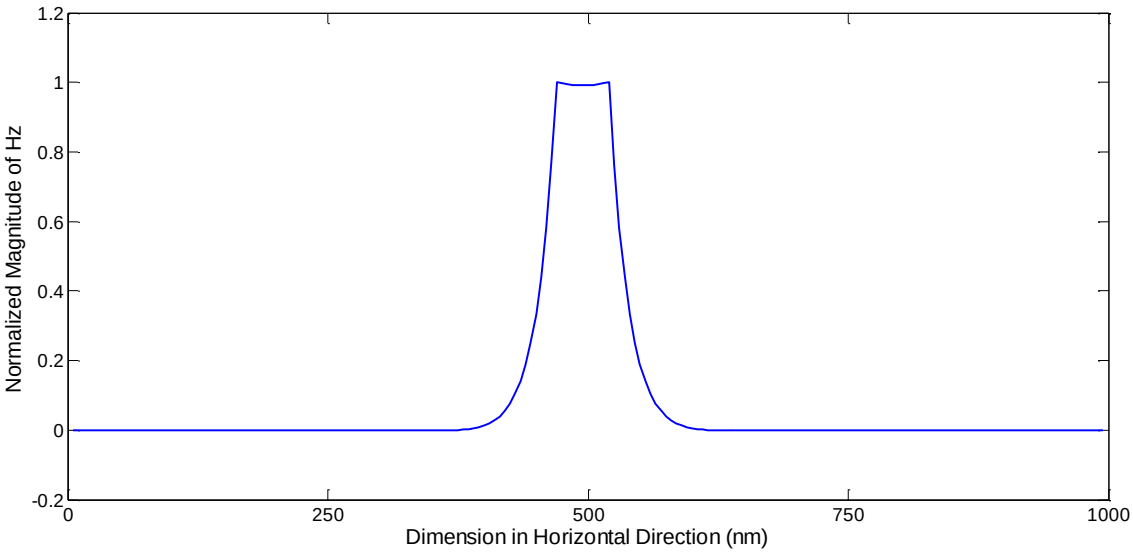

Fig.6.7: Hz fields for the generated plasmon propagation profile

Chapter 7

Performance Analysis of the Waveguides

7.1: Performance Analysis

7.1.1: Overview

MIM structures provide higher confinement on the other hand IMI structures facilitate longer propagation length. Relentless research is going on to investigate the tradeoff between confinement and propagation loss. For small corrugations losses are found to be very low while a high loss is expected with the gradual enlargement of corrugations .Herein, we emphasize on the output transmittance of an MIM waveguide with periodic grooves operating at an optical wavelength of 400nm to 2600nm. With a view to integrating the frequency dependent dispersive properties of materials in the FDTD algorithm, the essential parameters were attained.

7.1.2: Calculation of Energy at Output Port

For the purpose of calculating the energy, firstly the power for different time steps are calculated. To calculate the power at different time steps, Pyonting vector was used. Pyonting vector is defined as the cross product of Electric and Magnetic field intensities at a certain instant or here, time step. Mathematically-

$$\vec{\mathbf{S}} = \vec{\mathbf{E}} \times \vec{\mathbf{H}} \tag{7.1}$$

Where,

$\vec{\mathbf{S}}$ = instantaneous power,

$\vec{\mathbf{E}}$ = Electric field intensities

$\vec{\mathbf{H}}$ = Magnetic field intensities

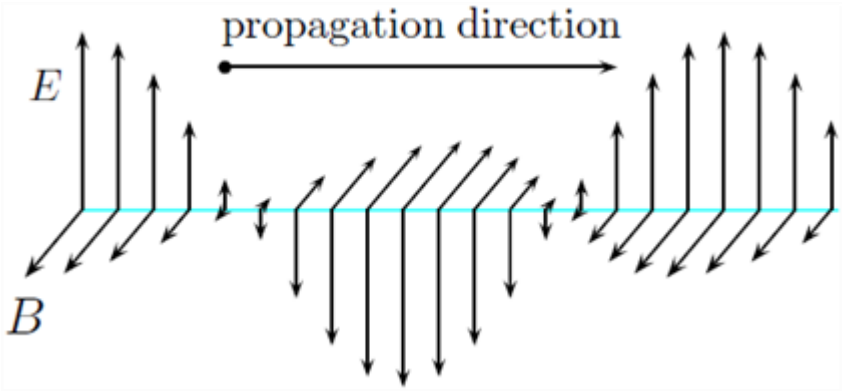

Fig 7.1: E and H fields for calculating instantaneous power.

The power over the range of calculated time steps is found out by multiplying with the time step, we can find out the total energy passed through a particular port for a given no. of time steps. Mathematically, energy passed through will be given by-

$$\mathbf{Energy} = |\overrightarrow{\mathbf{S}}| * \Delta\mathbf{t} \tag{7.2}$$

Where, $\Delta\mathbf{t}$ is the time step.

7.2: Performance of the Waveguides

7.2.1: Performance of the Waveguide with Variation of Corrugation Height

7.2.1.1: Transmission Spectra

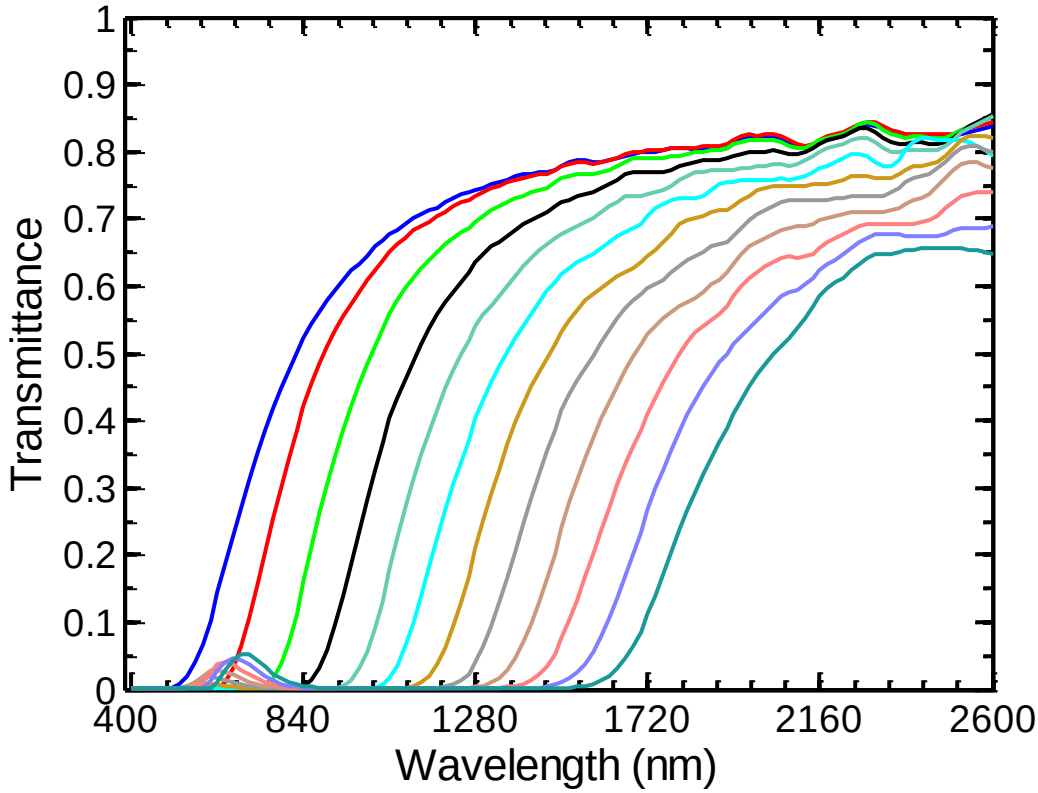

Fig.7.2. Output transmittance(or transmission spectra) with the variation of corrugation height(h) from 0nm to 55nm with an increment of 5nm.

7.2.1.2: Analysis of Spectra

Figure 7.1 represents the transmittance at different optical wavelengths for different corrugation height(h). It is seen from the graph that the cut off frequency shifts to the right with the gradual increment of the corrugation height(h). The transmittance of the propagated wave, for wavelengths less than the cut off wavelength, is almost zero.

7.2.2: Performance of the Waveguide with Variation of Corrugation Depth

7.2.2.1: Transmission Spectra

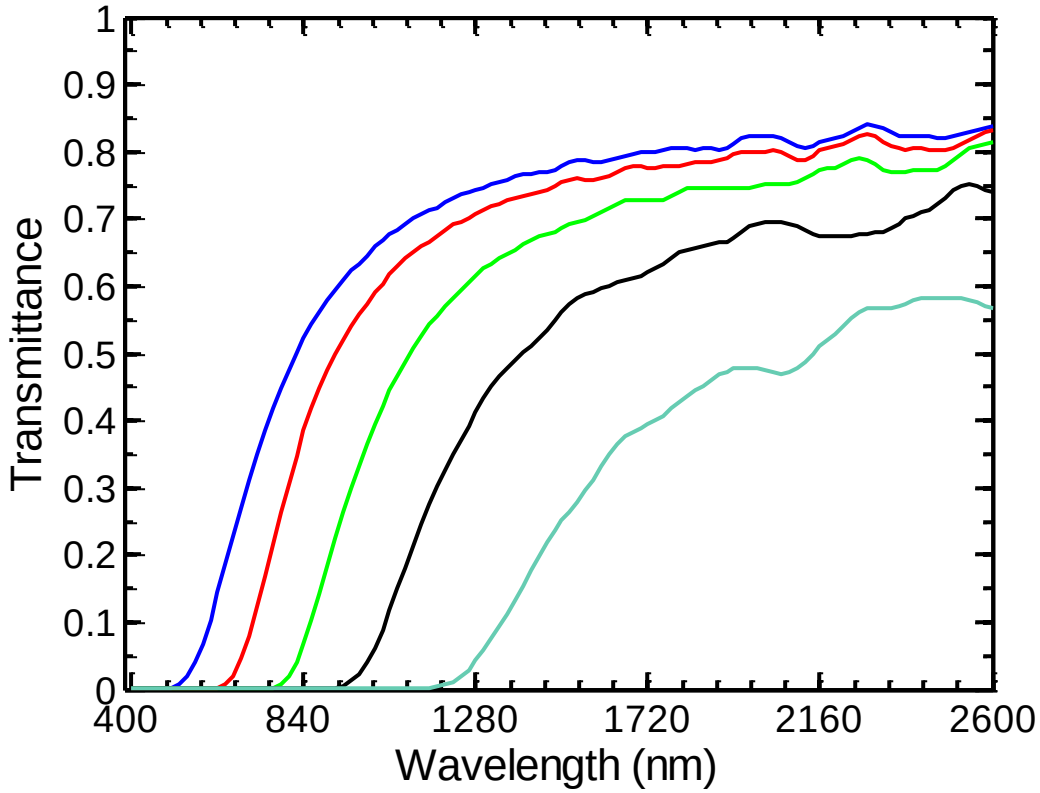

Fig.7.3. Output transmittance with the variation of corrugation depth(w) from 0nm to 20nm with an increment of 5nm.

7.2.2.2: Analysis of Spectra

Figure 5 shows the transmittance at different optical wavelengths as a function of corrugation depth(w). Meticulous FDTD simulations have established that the cut of wavelength moves towards right with the increase in corrugation depth(w).

7.2.3: Performance of the Waveguide with Variation of Both Corrugation Height and Depth

7.2.3.1: Transmission Spectra

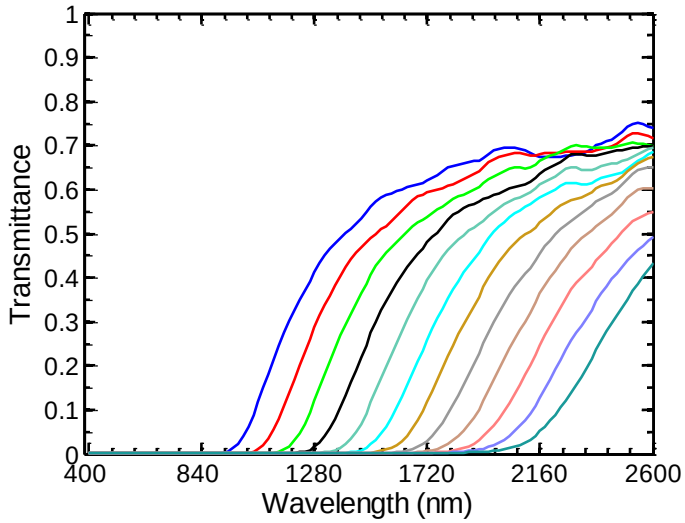

Fig.7.4. Output transmittance with the variation of corrugation height(h) from 0nm to 55nm with an increment of 5nm keeping the corrugation depth(w) fixed at 15nm.

7.2.3.2: Analysis of Spectra

Figure 6 displays the transmittance at different optical wavelengths for different corrugation heights(h) keeping the corrugation depth(w) fixed at 15nm. As can be observed from the graph, the cut of wavelength increases linearly with the increase in corrugation height(h). This structure offers a large range of cut off wavelengths with the compromise of a greater transmission loss. Note that all the structures behave like a high pass wavelength filter each possessing a unique range of cut off wavelengths.

Chapter 8

Conclusion

8.1: Conclusion

Our work can be summarized into the following points:

- Corrugated waveguide structures based on MIM surface plasmonic propagation has been investigated thoroughly.
- Transmission spectra for a wide range of wavelengths as a function of structure parameters such as corrugation height and depth has been simulated.
- The characteristics of a high pass filter is observed in all the grating structures.
- The investigation demonstrates that an adaptable cut off wavelength can be achieved by adjusting the structure parameters.
- This paper illustrates the idea of a plasmonic filter with grating structure for the manipulation of light at nanometric scale for integrated photonic devices.

Reference:

[1] W. L. Barnes, A. Dereux, and T. W. Ebbesen, "Surface plasmon subwavelength optics," Nature, vol. 424, pp. 824-830, 2003.

[2] S. A. Maier, Plasmonics: fundamentals and applications: Springer Science & Business Media, 2007.

[3] D. K. Gramotnev and S. I. Bozhevolnyi, "Plasmonics beyond the diffraction limit," Nature photonics, vol. 4, pp. 83-91, 2010.

[4] R. J. Blaikie and D. O. Melville, "Imaging through planar silver lenses in the optical near field," Journal of Optics A: Pure and Applied Optics, vol. 7, p. S176, 2005.

[5] D. Melville and R. Blaikie, "Super-resolution imaging through a planar silver layer," Optics Express, vol. 13, pp. 2127-2134, 2005.

[6] A. Hosseini and Y. Massoud, "A low-loss metal-insulator-metal plasmonic bragg reflector," Optics express, vol. 14, pp. 11318-11323, 2006.

[7] A. J. Haes and R. P. Van Duyne, "A nanoscale optical biosensor: sensitivity and selectivity of an approach based on the localized surface plasmon resonance spectroscopy of triangular silver nanoparticles," Journal of the American Chemical Society, vol. 124, pp. 10596-10604, 2002.

[8] J. Henzie, M. H. Lee, and T. W. Odom, "Multiscale patterning of plasmonic metamaterials," Nature nanotechnology, vol. 2, pp. 549-554, 2007.

[9] V. E. Ferry, L. A. Sweatlock, D. Pacifici, and H. A. Atwater, "Plasmonic nanostructure design for efficient light coupling into solar cells," Nano letters, vol. 8, pp. 4391-4397, 2008.

[10] S. Y. Chou and W. Ding, "Ultrathin, high-efficiency, broad-band, omni-acceptance, organic solar cells enhanced by plasmonic cavity with subwavelength hole array," Optics express, vol. 21, pp. A60-A76, 2013.

[11] S. A. Maier, "Plasmonics: Metal nanostructures for subwavelength photonic devices," Selected Topics in Quantum Electronics, IEEE Journal of, vol. 12, pp. 1214-1220, 2006.

[12] Han, Z., E. Forsberg, and S. He, Surface plasmon Bragg gratings formed in metal-insulator-metal waveguides. IEEE Photonics Technology Letters, 2007. **19**(2): p. 91-93.

[13] Jetté-Charbonneau, S., et al., Demonstration of Bragg gratings based on long ranging surface plasmon polariton waveguides. Optics express, 2005. **13**(12): p. 4674-4682.

[14] Boltasseva, A., et al., Integrated optical components utilizing long-range surface plasmon polaritons. Journal of Lightwave Technology, 2005. **23**(1): p. 413.

[15] Søndergaard, T., S.I. Bozhevolnyi, and A. Boltasseva, Theoretical analysis of ridge gratings for long-range surface plasmon polaritons. Physical Review B, 2006. **73**(4): p. 045320.

[16] M. D. Tocci, M. J. Bloemer, M. Scalora, J. P. Dowling, and C. M. Bowden, "Thin-film nonlinear optical diode," Applied physics letters, vol. 66, pp. 2324-2326, 1995.

[17] X.-S. Lin, J.-H. Yan, L.-J. Wu, and S. Lan, "High transmission contrast for single resonator based all-optical diodes with pump-assisting," Optics express, vol. 16, pp. 20949-20954, 2008.

[18] H. Zhou, K.-F. Zhou, W. Hu, Q. Guo, S. Lan, X.-S. Lin, et al., "All-optical diodes based on photonic crystal molecules consisting of nonlinear defect pairs," Journal of applied physics, vol. 99, p. 123111, 2006.

[19] S. F. Mingaleev and Y. S. Kivshar, "Nonlinear transmission and light localization in photonic-crystal waveguides," JOSA B, vol. 19, pp. 2241-2249, 2002.

[20] Zhu, J.H., et al., A nanoplasmonic high-pass wavelength filter based on a metal-insulator-metal circuitous waveguide. IEEE Transactions on Nanotechnology, 2011. **10**(6): p. 1357-1361.

[21] Pannipitiya, A., et al., Improved transmission model for metal-dielectric-metal plasmonic waveguides with stub structure. Optics express, 2010. **18**(6): p. 6191-6204.

[22] Yun, B., G. Hu, and Y. Cui, Theoretical analysis of a nanoscale plasmonic filter based on a rectangular metal–insulator–metal waveguide. Journal of Physics D: Applied Physics, 2010. **43**(38): p. 385102.

[23] E. Jin and X. Xu, "Plasmonic effects in near-field optical transmission enhancement through a single bowtie-shaped aperture," Applied Physics B, vol. 84, pp. 3-9, 2006.

[24] J. T. Krug II, E. J. Sánchez, and X. S. Xie, "Design of near-field optical probes with optimal field enhancement by finite difference time domain electromagnetic simulation," The Journal of chemical physics, vol. 116, pp. 10895-10901, 2002.

[25] W. H. Pernice, F. P. Payne, and D. F. Gallagher, "A general framework for the finite-difference time-domain simulation of real metals," Antennas and Propagation, IEEE Transactions on, vol. 55, pp. 916-923, 2007.

[26] A. D. Rakić, A. B. Djurišić, J. M. Elazar, and M. L. Majewski, "Optical properties of metallic films for vertical-cavity optoelectronic devices," Applied optics, vol. 37, pp. 5271-5283, 1998.

[27] M. A. Ordal, R. J. Bell, R. Alexander, L. Long, and M. Querry, "Optical properties of fourteen metals in the infrared and far infrared: Al, Co, Cu, Au, Fe, Pb, Mo, Ni, Pd, Pt, Ag, Ti, V, and W," Applied optics, vol. 24, pp. 4493-4499, 1985.

[28] G. Veronis and S. Fan, "Bends and splitters in metal-dielectric-metal subwavelength plasmonic waveguides," Applied Physics Letters, vol. 87, p. 131102, 2005.

[29] H. Gao, H. Shi, C. Wang, C. Du, X. Luo, Q. Deng, et al., "Surface plasmon polariton propagation and combination in Y-shaped metallic channels," Optics express, vol. 13, pp. 10795-10800, 2005.

[30] B. Wang and G. P. Wang, "Surface plasmon polariton propagation in nanoscale metal gap waveguides," Optics letters, vol. 29, pp. 1992-1994, 2004.

[31] G. Veronis and S. Fan, "Theoretical investigation of compact couplers between dielectric slab waveguides and two-dimensional metal-dielectric-metal plasmonic waveguides," Optics Express, vol. 15, pp. 1211-1221, 2007.

[32] P. Ginzburg and M. Orenstein, "Plasmonic transmission lines: from micro to nano scale with λ/4 impedance matching," Optics express, vol. 15, pp. 6762-6767, 2007.

[33] D. Pile and D. K. Gramotnev, "Adiabatic and nonadiabatic nanofocusing of plasmons by tapered gap plasmon waveguides," Applied Physics Letters, vol. 89, p. 041111, 2006.

[34] R. Wahsheh, Z. Lu, and M. Abushagur, "Nanoplasmonic air-slot coupler: design and fabrication," in Frontiers in optics, 2012, p. FTh4A. 6.

[35] R. Luebbers, F. P. Hunsberger, K. S. Kunz, R. B. Standler, and M. Schneider, “A frequencydependent finite-difference time-domain formulation for dispersive materials,” Electromagnetic Compatibility, IEEE Transactions on, vol. 32, no. 3, pp. 222–227, 1990.

[36] D. F. Kelley and R. J. Luebbers, “Piecewise linear recursive convolution for dispersive media using fdtd,” Antennas and Propagation, IEEE Transactions on, vol. 44, no. 6, pp. 792–797, 1996.

[37] R. J. Luebbers, F. Hunsberger, and K. S. Kunz, “A frequency-dependent finite-difference time-domain formulation for transient propagation in plasma,” Antennas and Propagation, IEEE Transactions on, vol. 39, no. 1, pp. 29–34, 1991.

[38] R. J. Luebbers and F. Hunsberger, “Fdtd for¡ e1¿ n¡/e1¿ th-order dispersive media,” Antennas and Propagation, IEEE Transactions on, vol. 40, no. 11, pp. 1297–1301, 1992.

[39] F. Hunsberger, R. Luebbers, and K. Kunz, “Finite-difference time-domain analysis of gyrotropic media. i. magnetized plasma,” Antennas and Propagation, IEEE Transactions on, vol. 40, no. 12, pp. 1489–1495, 1992

[40] F. Hunsberger, R. Luebbers, and K. Kunz, “Finite-difference time-domain analysis of gyrotropic media. i. magnetized plasma,” Antennas and Propagation, IEEE Transactions on, vol. 40, no. 12, pp. 1489–1495, 1992

[41] A. Akyurtlu and D. H. Werner, “Bi-fdtd: A novel finite-difference time-domain formulation for modeling wave propagation in bi-isotropic media,” Antennas and Propagation, IEEE Transactions on, vol. 52, no. 2, pp. 416–425, 2004

[42] A. Grande, I. Barba, A. C. Cabeceira, J. Represa, P. P. So, and W. J. Hoefer, “Fdtd modeling of transient microwave signals in dispersive and lossy bi-isotropic media,” Microwave Theory and Techniques, IEEE Transactions on, vol. 52, no. 3, pp. 773– 784, 2004.

[43] A. Akyurtlu and D. H. Werner, “A novel dispersive fdtd formulation for modeling propagation in chiral metamaterials,” Antennas and Propagation, IEEE Transactions on, vol. 52, no. 9, pp. 2267–2276, 2004